Optical technology for future telescopes

Kim, Dae Wook, Esparza, Marcos, Quach, Henry, Rodriguez, Stephanie, Kang, Hyukmo, et al.

Dae Wook Kim, Marcos Esparza, Henry Quach, Stephanie Rodriguez, Hyukmo Kang, Yi-Ting Feng, Heejoo Choi, "Optical technology for future telescopes," Proc. SPIE 11761, Fourth International Conference on Photonics and Optical Engineering, 1176103 (15 January 2021); doi: 10.1117/12.2586867

SPIE.

Event: Fourth International Conference on Photonics and Optical Engineering, 2020, Xi'an, China

Invited Paper

Optical Technology for Future Telescopes

Dae Wook Kim[a,b,c,*], Marcos Esparza[a], Henry Quach[a], Stephanie Rodriguez[a], Hyukmo Kang[a], Yi-Ting Feng[a], Heejoo Choi[a,c]

[a]Wyant College of Optical Sciences, Univ. of Arizona, 1630 E. University Blvd., Tucson, AZ 85721, USA
[b]Department of Astronomy and Steward Observatory, Univ. of Arizona, 933 N. Cherry Ave., Tucson, AZ 85721, USA
[c]Large Binocular Telescope Observatory, Univ. of Arizona, 933 N. Cherry Ave., Tucson, AZ 85721, USA

ABSTRACT

Various ground-based and space-based future telescope technologies are currently being conceptualized, designed, prototyped and tested to perform next generation astronomical sciences. They include (1) the alignment of segmented multi-order diffractive elements for the Nautilus space observatory; (2) the inflatable terahertz OASIS space telescope primary mirror characterization metrology; (3) active alignment of the laser truss-based Large Binocular Telescope prime focus camera; (4) the modular cross-dispersion spectroscopy unit, MOBIUS, used at the prime focal plane of the Large Binocular Telescope; (5) pupil segmentation topological optimization for future high contrast imaging telescopes; and (6) the optical design of the long slit UV spectroscopy space telescope Hyperion. This suite of enabling optical technologies and concept designs will redefine how humans understand the genesis and future of our universe.

Keywords: Optical Metrology; Telescope Alignment; Large Binocular Telescope; MOBIUS; OASIS; Nautilus; Hyperion; Pupil Segmentation

1. INTRODUCTION

The advancement of astronomical sciences is a key driver of engineering requirements for optical observatories. These requirements include technologies that allow for larger apertures in order to increase light collecting ability and resolution, the ability to multiplex optical signals via cross-dispersion and further optimization (e.g., pupil segmentation topology) of telescope and instrument design. Meeting these technology requirements pushes the overall science throughput of these observatories beyond that of existing ones. A series of new telescope and instrumentation concepts and designs are summarized and presented based on individual existing publications (with references to the original publications) in the context of future telescope technologies and solutions.

For more than a century, mirrors have been the standard optical element used for these large astronomical observatories, given their inherent achromatism and the fact that they are more lightweight than lenses of similar optical power and diameter. However, as mirrors for astronomical observation get larger and become segmented assemblies, the need to precisely figure and align them becomes much more stringent. The multi-order diffractive engineered (MODE) lens is a novel optical element that is lightweight, achromatic across a large spectrum and has more relaxed tolerances than mirror segments of a similar size [1]. The Nautilus Space Observatory concept provides a new solution utilizing transmissive MODE lens segments. [2] Our group has developed both a mechanism to align MODE lens segments [3] and an in-process metrology system to monitor the lens alignment while the segments are being bonded together. [4]

The Orbiting Astronomical Satellite for Investigating Stellar Systems (OASIS) is a terahertz space observatory that will explore the role of water in the evolution of planetary systems. OASIS features a 20-meter diameter primary mirror, which is obtained by using inflatable membrane technology. By pressurizing one transparent and one metallized membrane sealed around a rigid tensioning ring, a lenticular surface with immense light-collecting power can be obtained. [5] We present a metrology technique for measuring the surface figure of such novel inflatable mirrors. [6]

*dkim@optics.arizona.edu

Fourth International Conference on Photonics and Optical Engineering, edited by Jiangbo She,
Proc. of SPIE Vol. 11761, 1176103 · © 2021 SPIE · CCC code:
0277-786X/21/$21 · doi: 10.1117/12.2586867

Large ground-based telescopes are affected by environmental factors that can adversely affect image quality including mechanical deflections due to gravitational forces, thermal effects, and hysteresis. [7] To combat this, the Telescope Metrology System (TMS) is an active optics control system for large ground-based telescopes. TMS actively monitors and controls telescope collimation using a laser truss-based metrology method to determine the relative position and orientation of the telescopes primary mirror. TMS is under development for the Giant Magellan Telescope (GMT) and prototyped on the Large Binocular Telescope (LBT). [8] Currently, prototyping has progressed to TMS operation at prime focus between LBT's two 8.4m primary mirrors and the Large Binocular Camera (LBC).

The LUCI (LBT Utility Camera in the Infrared) instruments are a pair of near infrared (NIR) imagers and spectrographs for the LBT. [9, 10] Currently, we need both LUCIs simultaneously to get a spectrum covering the zJHK bands (zJ and HK). [11] MOBIUS (Mask-Oriented Breadboard Implementation for Unscrambling Spectra) is a novel expansion module to produce a simultaneous zJHK spectrum with a single LUCI. [12] By inserting the MOBIUS module, we extend simultaneous coverage down to 0.32 μm by binocular observations with one MODS (The Multi-Object Double Spectrographs) [13] and one LUCI.

A pinwheel aperture segmentation is another promising approach which obtains a Point Spread Function (PSF) with enhanced axial symmetry. Future very large aperture telescopes and high contrast imaging systems will utilize segmented optics including segment gaps and structural obscurations, which as a result, will produce diffraction effects that are disadvantageous to high contrast imaging (e.g., for exoplanet detection) or continuous wavefront control across the optical aperture. We present an optimization strategy for several pupil segment topologies for next-generation telescope concepts. Wave propagation results based on diffraction-limited point spread function analyses are modeled using Fraunhofer diffraction theory are presented using the Python-based POPPY simulation tool. [14 – 16]

The next generation UV space telescope concept, Hyperion, is designed to examine the origin of the stat formation. At the atomic-to-molecular interstellar boundary layer, the fuel for star formation (SF) is existed in a state of H2. [17 – 19] The observation of the edge of the interstellar reveal the secret of how a forming star impacts SF efficiency across galactic star-forming regions. The newly designed spectroscopy telescope, Hyperion, has been designed to observe the molecular interaction of star-forming clouds, the diffuse interstellar environment and new stars. Both the reflective telescope and cross-dispersion instrumentation design using freeform optics are presented.

2. FUTURE TELESCOPE DESIGNS AND INSTRUMENTS

2.1 Nautilus Space Observatory for Exoplanet Spectroscopy using Segmented Transmissive Optics

The Nautilus space observatory for exoplanet spectroscopy utilizes segmented transmissive lenses called MODE lenses. The alignment tolerances of a segmented MODE lens are on the order of micrometers rather than nanometers. However, new alignment technologies are still needed to reach these tolerances and meet engineering requirements specific to the MODE lens such as an unobscured aperture for use while bonding the lens segments.

Our group has been working on the Kinematically Engaged Yoke System (KEYS) to meet these technological challenges as shown in Figure 1. We designed a prototype to align the wedge segments of a 240-mm, diamond turned, PMMA MODE lens. KEYS uses the step-like features on the front face of the MODE lens to kinematically constrain the lens in five degrees of freedom with ball bearings bonded to the top of set screws shown in Figure 1(right), leaving the rotation of the wedge segments about the optical axis unconstrained. Folded flexures are used to adjust the wedge segment position in the remaining two degrees of freedom in the plane normal to the optical axis. [20] The set screws contacting the lens are used to adjust the wedge segments' tip, tilt and piston.

The KEYS was tested using a scanning white light interferometer (SWLI) and advanced deflectometry. The KEYS was able to align the wedge segments within 20 microns which is well within the tolerances needed for proper optical performance. The deflectometry system [21], which measured change in tip and tilt position after adjustment of the orientation of the lens segments, showed that the KEYS system was capable of a tip and tilt resolution of 0.006° (as seen in Figure 2) which is also within the needed tolerances. As we move forward with future versions of this alignment system, we will continue with the use of folded flexures for radial adjustment and kinematic contact using ball bearings as they have demonstrated the required performance to properly align a segmented MODE lens. [4]

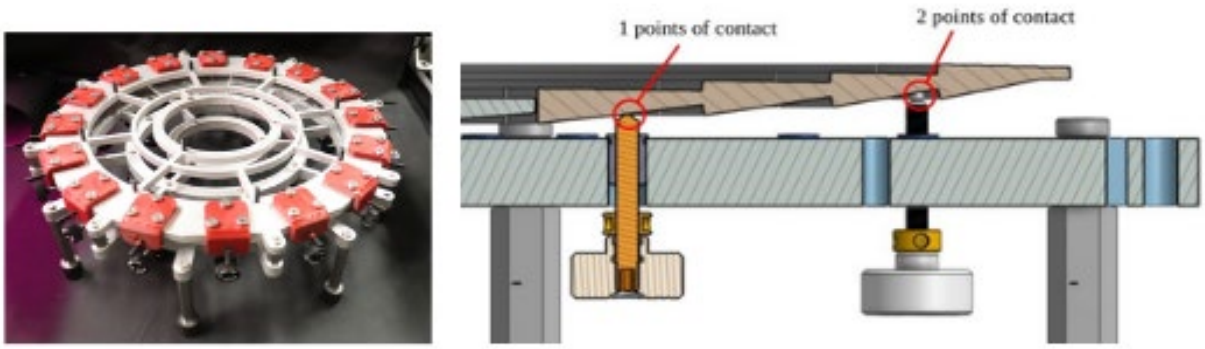

Figure 1. (left) The assembled KEYS prototype. (right) A cross-section view showing the contact points of the ball bearings on the step-like features of the MODE lens. [3]

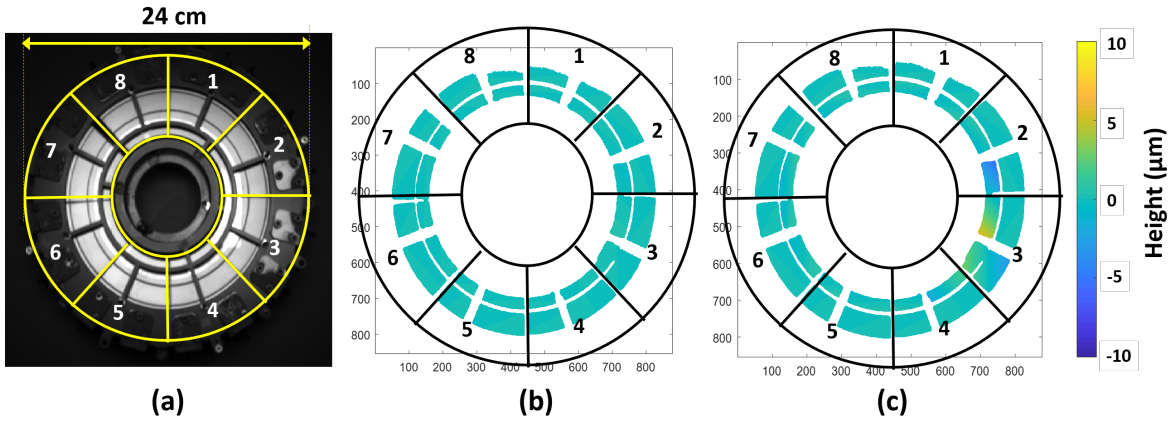

Figure 2. The real data from the metrology system (a) Live view from the camera. (b) All segments are well-aligned against initial co-phasing status. The black line represents the actual size of the single segment. It measures the unobscured area (from the KEYS structure), which is large enough to sense and monitor the misalignment. (c) Segment 3 drifted from the reference position and the measured tilting angle is 0.006°. (Note: The X and Y axis units of (b) and (c) are in pixels.) [4]

2.2 OASIS Terahertz Space Telescope using Inflatable 20 m Primary Mirror

The OASIS terahertz space telescope uses a unique inflatable 20 m primary mirror. [5] Despite knowing the inflated surface will take the general form of a Hencky curve Surface, factors such as variable inflation pressures, latent wrinkles, and the sheer aperture size make surface measurement challenging. It is essential for the chosen metrology technique to handle a wide dynamic range of surface slopes, which are expected during the membrane's iterative thermoforming treatment. Explorations of photogrammetry on a 1-meter OASIS model demonstrated that the depth of topically-printed fiducial dots could be reasonably obtained to the sample overall shape. However, a photogrammetric solution would be highly expensive in order to verifiably meet the 67-micron global accuracy requirements.

Alternatively, deflectometry was also explored to measure a 1-meter OASIS model as shown in Figure 3. [6] Deflectometry is a slope-measuring technique that can measure specular, concave optics without specialized hardware. Measurement is pixel-dense, requires only a standard camera and LCD display, and by nature of its ideal stigmatic configuration, obtains high slope measurement accuracy when the center of curvature is far from the aperture, such as in the 1-meter OASIS model and larger. To demonstrate the versatility of this technique, we obtained 8 measurements of different inflation pressures in rapid succession, showing the shape change of the optical surface as it varied several hundred millimeters in focal length. Obtaining global accuracy in deflectometry measurement is a matter of calibrating the global coordinates of the aperture to the camera and screen once with a laser tracker. The OASIS team will use both photogrammetry and deflectometry to verify surface shape across various pressures and thermoforming treatments.

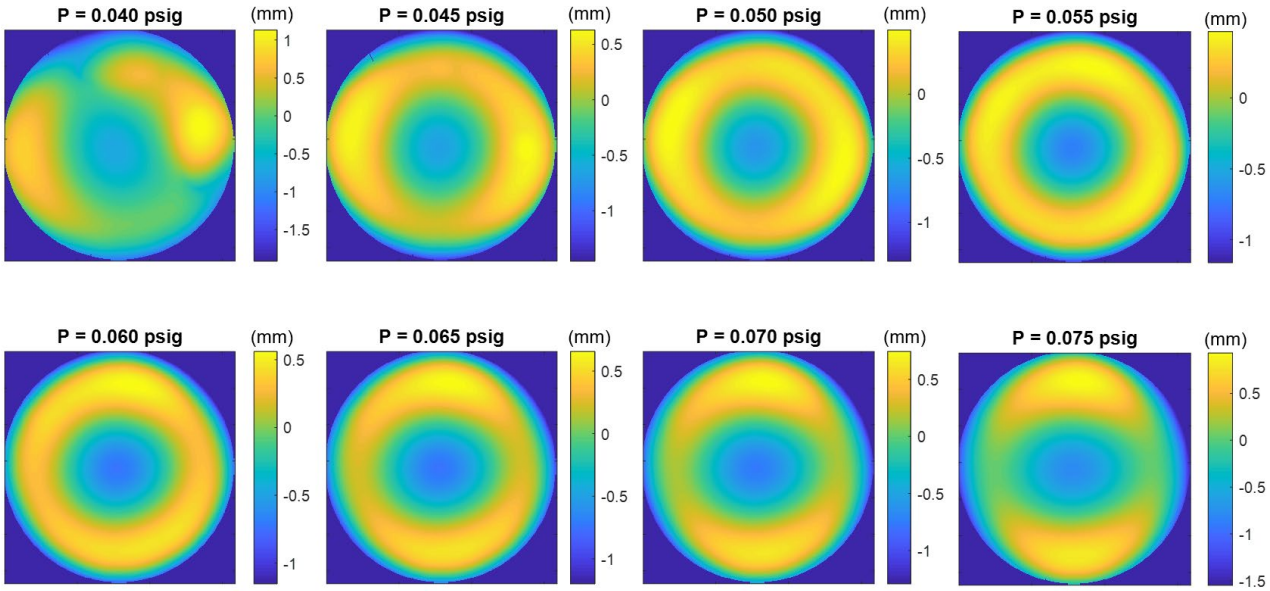

Figure 3. The shape of the inflatable 1-meter OASIS model optic is observed from a top view of the full aperture, shown with Z1-Z4 removed. At lower pressures, stress is less evenly distributed across the aperture, so the radial non-uniformity is more pronounced. At higher pressures, the presence of astigmatism arises from the differing mechanical properties of the orthotropic membrane material. The acquisition and full processing of all of the ~600 × 600 pixel maps shown took less than an hour total, once system calibration was established. [6]

2.3 Large Binocular Telescope Prime Focus Camera Alignment using Laser Truss Alignment System

The LBT team is developing a laser truss alignment system [7]. A laser truss is created between the primary mirror and the prime focus camera LBC. The laser truss is composed of the measurement arms of the TMS system that extend from collimators around the primary mirror to retroreflectors on LBC as shown in Figure 4. An absolute distance measuring interferometer, the Etalon Absolute Multiline Technology (EAMT), simultaneously measures the laser truss leg lengths with micron level accuracy. An inverse kinematic analysis of EAMT laser truss leg measurements determines the relative position and orientation of the primary mirror.

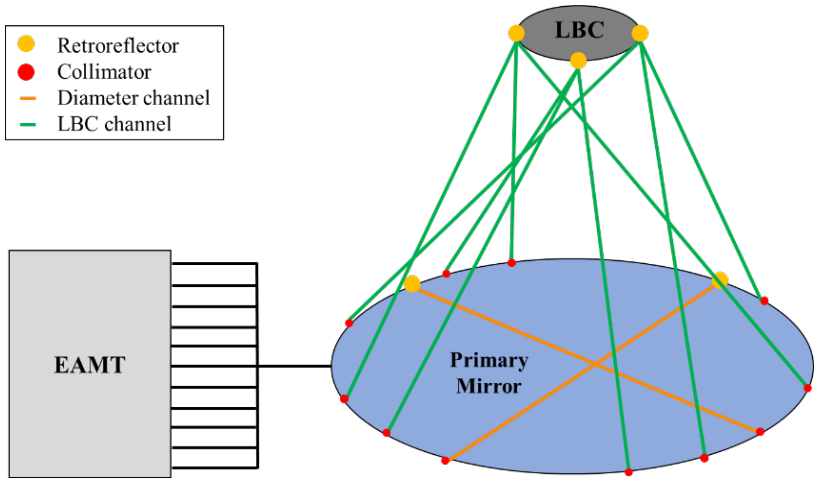

Figure 4 Laser truss configuration on LBT. The EAMT fiber channels extend to the collimators around the primary mirror. Each of the three retroreflectors on LBC have three collimators aligned to create the laser truss. There are two measurement channels that monitor the diameter of the mirror. [7]

The relative position and orientation of the primary mirror as determined by TMS was validated using controlled incremental motion of the primary mirror. The full range of motion for normal telescope operation was tested the results for induced Rx motion are shown in Figure 5. The calculated pose showed a maximum deviation from telescope controls for the given set of data of 1.7 μm for lateral motion and 0.1 arcsec for rotational motion, which are within the expected range or deviation.

The primary mirror position and orientation data from TMS is then input into an optical model to iteratively perform aberration and image quality analysis. Zernike coefficients for first order coma are determined using TMS data taken over controlled Rx motion is shown in Figure 5. On-axis and off-axis fields were considered. The field is increased parallel to Z7 coma. Field dependence is exhibited as Z7 shifts in magnitude at an off-axis field position. Z8 has no field dependence and does not shift at off axis field positions since it is oriented perpendicular to the increase in field. [7]

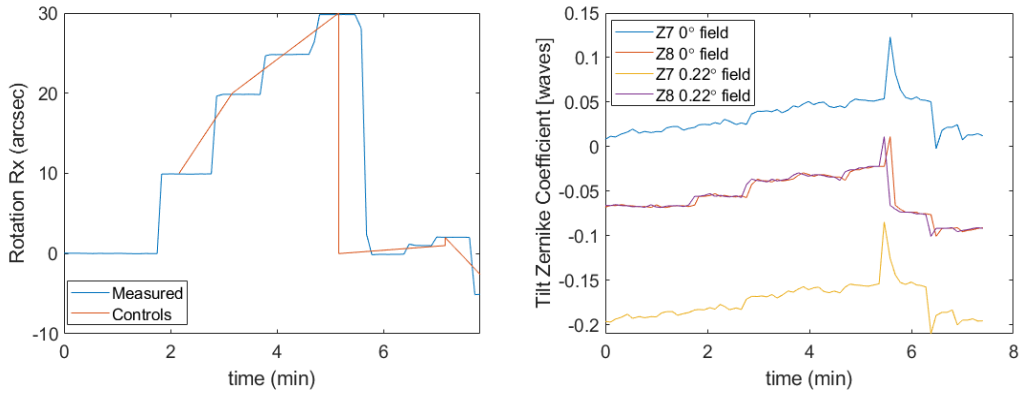

Figure 5 TMS data was validated using controlled Rx motion of the primary mirror (left). Zernike terms for horizontal and vertical first order coma is shown for on-axis and off-axis fields (right) [7].

2.4 MOBIUS: Large Binocular Telescope Modular Cross-Dispersion Instrument

MOBIUS is a plug-in cross-disperser module which will be installed inside of an exchangeable slit mask frame of LUCI. The MOBIUS-equipped slit mask frame will be located at the focal plane of the LBT and the module disperses the input slit image perpendicular to the dispersion direction of the gratings in LUCI. MOBIUS enables a single LUCI to produce a simultaneous zJHK spectrum yet requires no modification to the current set up of LUCI (Figure 6).

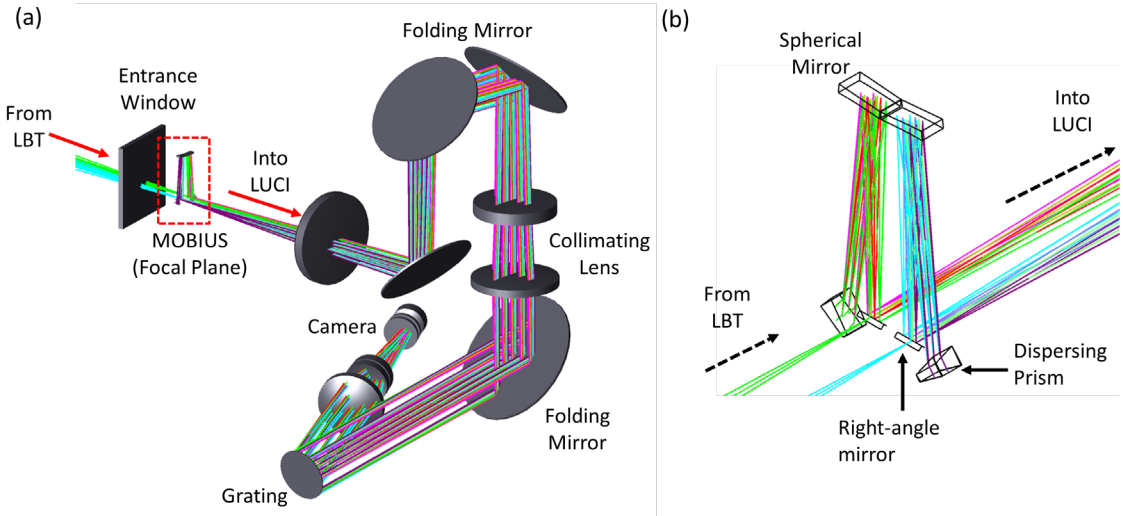

Figure 6. (a) Overall layout of LUCI with MOBIUS. MOBIUS-equipped frame substitutes one of the traditional slit frame mask and consequently no modifications are needed in current instrument settings. (b) Optical layout of MOBIUS. Two identical spectrograph units are located side by side for the sky subtraction by dithering. [12]

Figure 7 shows that MOBIUS can expand wavelength coverage of LUCI with little penalty. MOBIUS-equipped LUCI generates zJHK spectra in a single shot without overlap while allowing a slit length up to 2.3 arcseconds. Also, MOBIUS induces less than a pixel of change in half width distance for 90% fraction of ensquared energy on detector. This change is negligible as the smallest expected seeing disk size is larger than 150 μm (2 pixels) or 0.25 arcseconds.

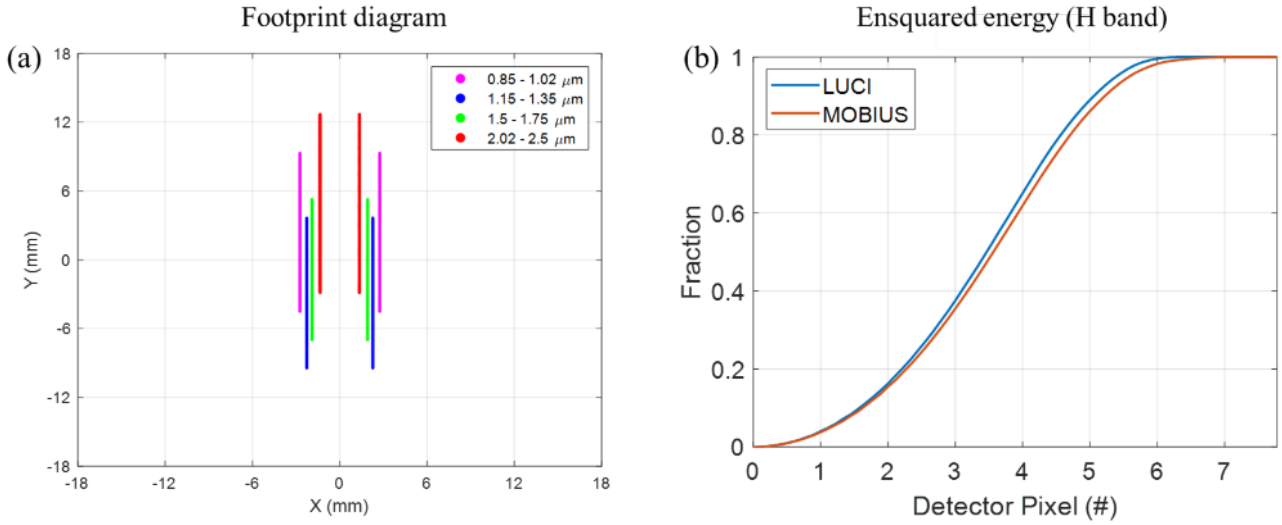

Figure 7. (a) Footprint diagram at the detector when observing LUCI with MOBIUS. We can acquire zJHK spectras simultaneously without overlap. (b) Ensquared energy comparison between LUCI and LUCI with MOBIUS in H band. [12]

2.5 Large Aperture Pinwheel Pupil Telescope for Axially Symmetric Point Spread Function

Most modern segmented mirror designs have been either hexagonal or circular, but more options for future telescopes are explored and presented in Figure 8. Each pupil creates different footprint on the PSF image in the focal plane, shown in Figure 9. Among them, hex-segmented, keystone, and pinwheel pupil [22] were selected to compare their PSF images among several criteria. A hex-segmented pupil has much higher irradiance spikes but also appears to have significant regions of lower irradiance, and the range between such spikes and low region spans from 10^{-17} to 10^{-6}. [16] The pinwheel pupil doesn't have such a min-max region but provides more uniform irradiance distribution both in the bright rings and the dark rings of PSF, which could improve the performance of active wavefront control for exoplanet imaging and decrease confusion in crowded astronomical fields such as star clusters. The possibility of hiding the dim light from an exoplanet can be decreased as well.

A pinwheel pupil can smooth and spread out the "beading effect" azimuthally on the PSF image by curving the straight edges to curved ones. This can prevent the straight flares spanning from the center of the PSF to the outer rings, the PSF thus appears more like an Airy disk. The tolerance analysis is performed comparing pinwheel pupil and hexagonally segmented pupil, including 2-D displacement, rotation, and edge manufacture error of segments. It is demonstrated that hexagonally segmented pupil performance has a high sensitivity to edge piston error as the deep dark degrades significantly. The Min profiles rise in an order of at least 10^2 with a small error in segment misalignment and rotation. The same conditions are applied to a Pinwheel pupil, which also raises the min profiles about 10^3. However, this is actually beneficial for a Pinwheel pupil. The raised min profile reduces the range between max and min profiles, further flattening, or smoothing the irradiance along each ring of the PSF pattern, which approaches a perfect Airy disk.

The fundamental and important topological analysis presented is expected to provide a guideline for next-generation telescope primary mirror segmentation and secondary spider design. The further investigation of integrating a pinwheel aperture to a vector vortex coronagraph (e.g., VV6 or VV8) system for HabEx remains to be studied. Intuitively, the advantage of using a pinwheel pupil with a coronagraph offers very flexible and phenomenal solution, creating an Airy Disk-like PSF pattern, which can serve as a great alternative for future space missions.

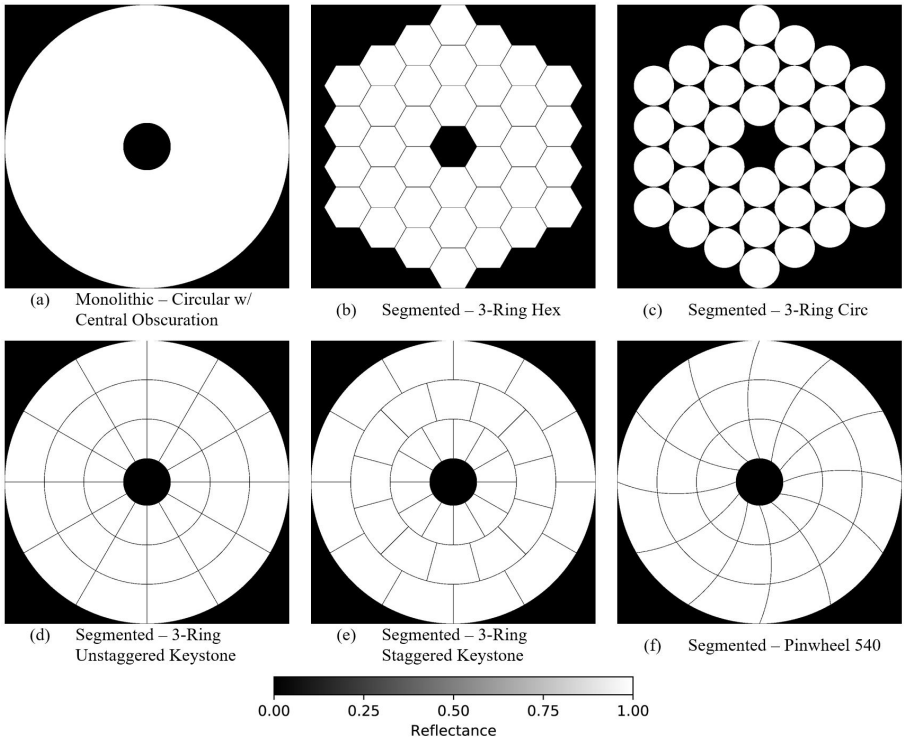

Figure 8. Illustration of the segmented pupil topologies. Each pupil has the same aperture diameter of 12 m. The white is the mirror's reflecting surface, and black shows the obscured area. (Note: segment gap width is set to 20 mm.) [16]

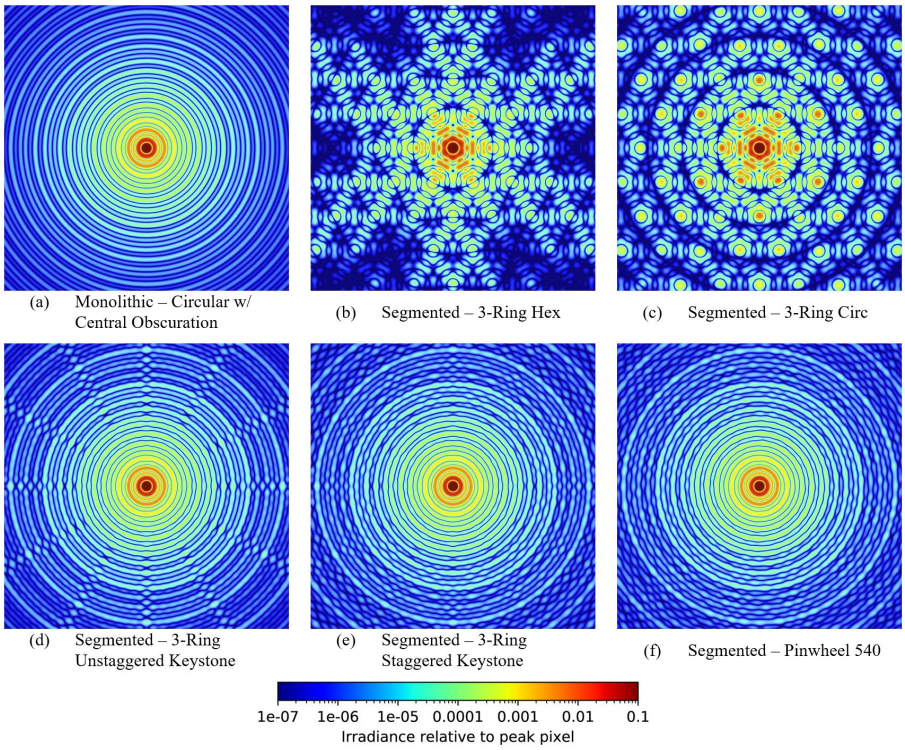

Figure 9. Illustration PSFs within 1 arcsec field of view for each of the pupils listed in Figure 8, calculated at wavelength 1μm. The PSFs are all in log scale with color bar at the bottom indicated the value. [16]

2.6 Hyperion Space Telescope for Far-UV Cross Dispersion Spectroscopy

With its updated design, the far-UV space telescope Hyperion has adopted a significantly longer slit length. The extreme aspect ratio of the long-slit (10 arcmin × 2.5 arcsec, F/6, EFL = 2400 mm) and the very high spectral resolution requirement (R > 30,000) at the FUV spectral range (1405 Å – 1645 Å) make the optical design of Hyperion unique by utilizing the freeform imaging optics and échelle cross-dispersion configuration design approach as shown in Figure 10.

The Ritchey-Chrétien telescope design (i.e., hyperbolic mirror for primary and secondary) is adopted to cover relative wide 10 arcmin field of view of slit width and it converges F/6 beam to the spectrometer section. The aberration of long slit imaging was resolved by using annular type échelle grating and placing the slit on-axis of the telescope to create a normal incidence angle to the échelle grating, as shown in Figure 10 (a) without any photon loss and obstacle.

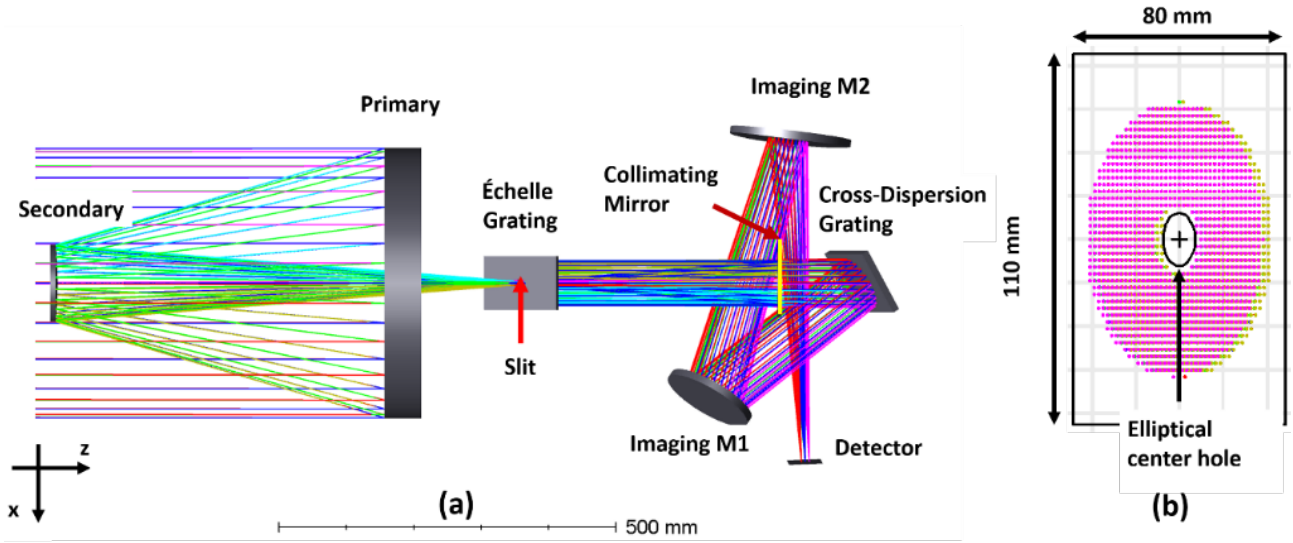

Figure 10. The schematic diagram of Ritchey-Chrétian telescope, consecutive cross-dispersion grating, and Type-4 form imaging optics. (a) In order for low aberration with long slit imaging, the slit is placed at the échelle grating center hole. The diffraction angle of the échelle and cross-dispersion are orthogonal to each other. (b) Annular type échelle grating with a central hole (matching the secondary mirror obscuration) allows the unique on-axis optical layout without photon loss. [17]

We have published the smart layout of Type-4 design that could accommodate a large field while minimum aberration. [17] The freeform two-mirror imaging system (M1 and M2) was adopted to have small spots on the sensor plane and to have high spectral resolution. It has the benefit of a large FOV and a small volume, and those are critical factor for this mission. The on-axis layout of all dispersive series elements reduces the off-axis aberration. [23, 24] The M1 and M2 in Type-4 design are optimized with Zernike polynomials and it also well accommodate the separated pupil matching of two grating planes.

3. CONCLUDING REMARKS

A diverse selection of ground-based and space-based next generation telescope technologies are actively being conceptualized, designed, prototyped, and demonstrated. This suite of optical technologies serves the next generation of astronomical investigations by offering novel yet applicable approaches that the wider design and engineering community can practically use. It is our hope that these contributions in design and instrumentation will not only provide new practical benchmarks for modern astronomy today, but also precipitate the next great insights and questions about our universe.

ACKNOWLEDGEMENT

The authors would like to acknowledge the Gordon and Betty Moore Foundation for their financial support of the development of the MODE lens and its enabling alignment technologies. Also, we would like to acknowledge the II-VI Foundation Block-Gift, Technology Research Initiative Fund Optics/Imaging Program, and Friends of Tucson Optics Endowed Scholarships in Optical Sciences for helping support the optical design and metrology research conducted in the LOFT group.

REFERENCES

[1] Y. Kim, Z. Wang, and T. Milster, "Ultralight Very Large Aperture Space Telescopes using MODE Lens Technology," in *Optical Design and Fabrication 2019 (Freeform, OFT)*, 2019, p. FM4B.4, doi: 10.1364/FREEFORM.2019.FM4B.4.

[2] D. Apai *et al.*, "A Thousand Earths: A Very Large Aperture, Ultralight Space Telescope Array for Atmospheric Biosignature Surveys," *Astron. J.*, 2019, doi: 10.3847/1538-3881/ab2631.

[3] M. A. Esparza, H. Choi, and D. W. Kim, "Alignment of Multi-Order Diffractive Engineered (MODE) lens segments using the Kinematically-Engaged Yoke System," in *Proc.SPIE*, Aug. 2020, vol. 11487, doi: 10.1117/12.2569442.

[4] H. Choi *et al.*, "In-process metrology for segmented optics UV curing control," in *Proc.SPIE*, Aug. 2020, vol. 11487, doi: 10.1117/12.2569310.

[5] C. Walker *et al.*, "Orbiting Astronomical Satellite for Investigating Stellar Systems (OASIS)," 2019.

[6] H. Quach *et al.*, "Full-aperture optical metrology for inflatable membrane mirrors," in *Proc.SPIE*, Aug. 2020, vol. 11487, doi: 10.1117/12.2569750.

[7] S. Rodriguez *et al.*, "Implementation of a laser-truss based telescope metrology system at the Large Binocular Telescope," in *Proc.SPIE*, Aug. 2020, vol. 11487, doi: 10.1117/12.2576438.

[8] A. Rakich *et al.*, "Prototyping the GMT telescope metrology system on LBT," in *Proc.SPIE*, Jul. 2018, vol. 10700, doi: 10.1117/12.2313900.

[9] W. Seifert *et al.*, "LUCIFER: a multimode NIR instrument for the LBT," in *Proc.SPIE*, Mar. 2003, vol. 4841, doi: 10.1117/12.459494.

[10] H. Mandel *et al.*, "LUCIFER status report: summer 2008," in *Proc.SPIE*, Jul. 2008, vol. 7014, doi: 10.1117/12.787203.

[11] B. Rothberg *et al.*, "Current status of the facility instruments at the Large Binocular Telescope Observatory," in *Proc.SPIE*, Jul. 2018, vol. 10702, doi: 10.1117/12.2314005.

[12] H. Kang, D. Thompson, A. Conrad, C. Vogel, A. Lamdan, and D. W. Kim, "Modular plug-in extension enabling cross-dispersed spectroscopy for Large Binocular Telescope," 2019, doi: 10.1117/12.2528865.

[13] R. W. Pogge *et al.*, "The multi-object double spectrographs for the Large Binocular Telescope," 2010, doi: 10.1117/12.857215.

[14] E. S. Douglas and M. D. Perrin, "Accelerated modeling of near and far-field diffraction for coronagraphic optical systems," 2018, doi: 10.1117/12.2313441.

[15] M. Perrin, J. Long, E. Douglas, A. Sivaramakrishnan, C. Slocum, and others, "POPPY: Physical Optics Propagation in PYthon," Astrophysics Source Code Library ascl:1602.018 (2016).

[16] Yi-Ting Feng, Jaren Nicholas Ashcraft, James B. Breckinridge, James E. Harvey, Ewan S. Douglas, Heejoo Choi, Charles Lillie, Tony Hull, and Dae Wook Kim, "Topological Pupil Segmentation and Point Spread Function Analysis for Large Aperture Imaging Systems," Proc. SPIE, AOPC 2020 Conference Beijing, China (2020). (In press)

[17] H. Choi, I. Trumper, Y.-T. Feng, H. Kang, E. Hamden, and D. W. Kim, "Hyperion: Far-UV cross dispersion spectroscope design," in *Proc.SPIE*, Aug. 2020, vol. 11487, doi: 10.1117/12.2570489.

[18] D. Decataldo, A. Pallottini, A. Ferrara, L. Vallini, and S. Gallerani, "Photoevaporation of Jeans-unstable molecular clumps," *Mon. Not. R. Astron. Soc.*, vol. 487, no. 3, pp. 3377–3391, Aug. 2019, doi: 10.1093/mnras/stz1527.

[19] M. R. Krumholz, "The big problems in star formation: The star formation rate, stellar clustering, and the initial mass function" *Physics Reports.* 2014, doi: 10.1016/j.physrep.2014.02.001.

[20] S. Awtar, A. H. Slocum, and E. Sevincer, “Characteristics of beam-based flexure modules,” *J. Mech. Des. Trans. ASME*, 2007, doi: 10.1115/1.2717231.
[21] H. Choi, I. Trumper, D. W. Kim, M. Dubin, and W. Zhao, “Simultaneous angular alignment of segmented mirrors using sinusoidal pattern analysis,” 2017, doi: 10.1117/12.2275197.
[22] J. B. Breckinridge, J. E. Harvey, K. Crabtree, and T. Hull, “Exoplanet telescope diffracted light minimized: the pinwheel-pupil solution,” in *Proc.SPIE*, Jul. 2018, vol. 10698, doi: 10.1117/12.2311811.
[23] W. J. Smith, *Modern lens design*, 2nd ed. New York: New York : McGraw-Hill, 2005.
[24] R. R. Shannon, *The Art and Science of Optical Design*. West Nyack: West Nyack: Cambridge University Press, 1997.